

ULTRA-LUMINOUS X-RAY SOURCES AS SUPER-CRITICAL PROPELLERS

M. HAKAN ERKUT¹, K. YAVUZ EKŞİ¹, M. ALI ALPAR²

¹ Istanbul Technical University, Faculty of Science and Letters, Physics Engineering Department, 34469, Istanbul, Turkey
and

² Sabancı University, Orhanlı Tuzla, 34956 İstanbul, Turkey

ABSTRACT

We study the evolution of newborn neutron stars in high-mass X-ray binaries interacting with a wind-fed super-Eddington disk. The inner disk is regularized to a radiation-dominated quasi-spherical configuration for which we calculate the inner radius of the disk, the total luminosity of the system and the torque acting on the neutron star accordingly, following the evolution of the system through the ejector and early propeller stages. We find that the systems with $B \gtrsim 10^{13}$ G pass through a short (~ 20 yr) ejector stage appearing as supernova impostors followed by a propeller stage lasting $\sim 10^3$ yr. In the super-critical propeller stage the system is still bright ($L \sim 10^{40}$ erg s⁻¹) due to the spindown power and therefore appears as an ultra-luminous X-ray source (ULX). The system evolves into pulsating ULX (PULX) when the neutron star spins down to a period ($P \sim 1$ s) allowing for accretion onto its surface to commence. Systems with lower magnetic fields, $B \sim 10^{11}$ G, pass through a long (10^5 yr) super-critical propeller stage with luminosities similar to those of the ultra-luminous super-soft sources (ULS), $L \lesssim 10^{40}$ erg s⁻¹. The equilibrium periods of these systems in the accretion stage is about 10 ms, which is much smaller than the typical period range of PULX observed to date. Such systems could have a larger population, but their pulsations would be elusive due to the smaller size of the magnetosphere. Our results suggest that the ULS and some nonpulsating ULX are rapidly spinning and highly magnetized young neutron stars at the super-critical propeller stage.

Keywords: stars: neutron — X-rays: binaries — accretion, accretion disks

1. INTRODUCTION

The recent detection of pulsations from four ultra-luminous X-ray sources (ULX; [Bachetti et al. 2014](#); [Israel et al. 2017a,b](#); [Fürst et al. 2016](#); [Carpano et al. 2018](#)) not only showed that a large fraction of these objects could be hosting neutron stars ([Shao & Li 2015](#); [Wiktorowicz et al. 2015, 2017](#); [King et al. 2017](#); [Middleton & King 2017](#)) accreting matter from a companion object but also that the stellar-mass objects could exceed the classical Eddington limit.

Another subclass of ULX are the ultra-luminous super-soft sources (ULS) characterized by very soft X-ray spectra $k_B T = 0.05 - 0.2$ keV ([Di Stefano & Kong 2003](#); [Fabbiano et al. 2003](#); [Kong & Di Stefano 2003](#)) whereas the conventional ULX have a better part of their luminosity above 1 keV. ULX are possibly a heterogeneous class, PULX and ULS' forming subclasses. It is argued that the differences between conventional ULX and ULS' simply arise from our viewing angle, ULS being observed at high inclination angles (edge on) so that a thicker layer of material is obscuring the central engine ([Kylafis & Xilouris 1993](#); [Poutanen et al. 2007](#); [Feng](#)

[et al. 2016](#); [Urquhart & Soria 2016](#); [Pinto et al. 2017](#)).

X-ray spectra of PULX are similar to those of most ULX ([Pintore et al. 2017](#)). Although it is more likely that the compact objects in most ULX are neutron stars, the lack of pulsations is addressed by the likely presence of an optically thick envelope that smears out the pulsations ([Ekşi et al. 2015](#); [Mushtukov et al. 2017](#)). Recently, it was shown by [Tsygankov et al. \(2016\)](#) that the first detected PULX, M82 X-2, has a bimodal luminosity distribution likely because the system occasionally enters into a propeller stage ([Illarionov & Sunyaev 1975](#)) when the matter cannot accrete onto the star due to centrifugal barrier. It is then natural to think that some ULX could be systems at an early evolutionary epoch in which the neutron star is rotating much faster than a critical rotation rate and is spinning down rapidly, far from spin equilibrium. In the super-critical (super-Eddington) mass influx regime expected for the ultra-luminous sources the propeller can easily facilitate outflows and winds from the disk ([Lovelace et al. 1999](#)).

In this paper, we advance the view that a fraction of the ULX/ULS population are strongly magnetized

$B \sim 10^{11} - 10^{13}$ G neutron stars at the super-critical propeller stage (Lipunov 1982; Mineshige et al. 1991; Lipunova 1999). In this picture, the spindown energy transferred to the wind-fed disk is the main source of energy at initial stages. Given the evidence for the presence of disks and optically thick outflows, it is likely that some of these objects are spinning down under propeller torques from quasi-spherical wind-fed disks. In our picture, ULX/ULS systems with $B \gtrsim 10^{13}$ G, (a system with the same properties is seen as a ULX or ULS, depending on the viewing angle) are progenitors of PULX i.e. they would become PULX when the neutron star slows down sufficiently. Mass flow toward the neutron star proceeds by wind at the earliest stages of evolution associated with ULX and ULS depending on the dipole magnetic field of the neutron star, but at some stage Roche-lobe overflow commences. This view is consistent with the recent understanding that any ULX system represents a short-lived phase in the life of a binary system (King et al. 2001; Wiktorowicz et al. 2015).

The structure of this paper is as follows: In Section 2, we introduce the basic concepts and equations to derive the spindown torque on the neutron star acting as a supercritical propeller and the luminosity of the disk around this propeller. We present the results of our analysis in Section 3. In Section 4, we discuss the astrophysical implications of ULXs being super-critical propellers.

2. THE SUPER-CRITICAL PROPELLER

The condition for disk formation is that the specific angular momentum of stellar wind matter be larger than the specific angular momentum of matter in Keplerian orbit at the magnetopause (Iben et al. 1995; Lü et al. 2011). This requires the relative velocities between the neutron star and the wind to be smaller than those expected for radiatively driven winds. Smaller wind velocities can be due to ionization by the X-ray source and wind flows concentrated toward the neutron star if the optical companion is close to filling its Roche lobe (Livio et al. 1986). Even if the wind matter falls quasi-radially toward the neutron star and thus carries little net angular momentum, a disk can form at the rotation equator following the transfer of angular momentum from the neutron-star magnetosphere to the infalling gas (Anzer et al. 1987). In what follows, we assume that the mass donor transfers matter at supercritical rates $\dot{M}_0 > \dot{M}_E \equiv L_E/\epsilon c^2$, throughout the wind-fed disk around the newborn rapidly rotating neutron star in some ULX/ULS systems. Here, $L_E = 4\pi GMm_p c/\sigma_T$ is the Eddington luminosity, $\epsilon \simeq 0.1$ is the efficiency of gravitational energy release, m_p is the proton mass, c is the speed of light, and σ_T is the Thomson cross-section of the electron.

2.1. Basic concepts

The propeller stage is realized when the neutron star rotates so fast that mass cannot be accreted onto the star due to the centrifugal barrier (Illarionov & Sunyaev 1975). This condition is satisfied when the inner radius of the disk, R_{in} , is greater than the corotation radius, $R_{\text{co}} = (GM/\Omega_*^2)^{1/3}$, where M is the mass and Ω_* is the angular rotation frequency of the neutron star (Lovelace et al. 1999). The system is in the super-critical propeller stage (Lipunov 1987) if matter is transferred from the donor at a super-critical rate ($\dot{M}_0 > \dot{M}_E$) while the corotation radius remains smaller than the inner radius of the disk because of the rapid rotation of the neutron star.

The super-critical mass transfer within the disk leads to the spherization of the disk within a critical radius,

$$R_{\text{sp}} = \frac{27\epsilon\sigma_T\dot{M}_0}{8\pi m_p c} \simeq 1.43 \times 10^9 \text{ cm } \epsilon \left(\frac{\dot{M}_0}{10^{20} \text{ g s}^{-1}} \right), \quad (1)$$

determined by $L(R > R_{\text{sp}}) = 27\epsilon GM\dot{M}_0/2R_{\text{sp}} = L_E$ (Shakura & Sunyaev 1973). The flow regulates itself so that some of the matter within the spherization radius is ejected from the system with a radiation-dominated outflow

$$\dot{M} = \begin{cases} \dot{M}_0 (R/R_{\text{sp}}), & \text{for } R < R_{\text{sp}}; \\ \dot{M}_0, & \text{for } R > R_{\text{sp}}. \end{cases} \quad (2)$$

(Shakura & Sunyaev 1973). Accordingly, the mass flux within the disk is regulated not to exceed the Eddington limit too much, but only logarithmically: $L \simeq L_E[1 + \ln(\dot{M}_0/\dot{M}_E)]$ (Shakura & Sunyaev 1973).

2.2. Angular Momentum Loss From the System

A young strongly magnetized neutron star enshrouded in super-critical flow would spindown at a very high rate. We assume that the angular momentum also is lost with the outflows. For consistency with Equation 2 we write

$$j = \begin{cases} \dot{J}_0 (R/R_{\text{sp}})^{3/2}, & \text{for } R < R_{\text{sp}}; \\ \dot{J}_0, & \text{for } R > R_{\text{sp}}. \end{cases} \quad (3)$$

Here,

$$\dot{J}_0 = \dot{M}R^2\Omega + 2\pi R^3\eta \frac{d\Omega}{dR} \quad (4)$$

is the angular momentum flux through the radius $R > R_{\text{sp}}$ of the disk whose radial size is limited by R_0 and η is the vertically integrated dynamical viscosity. Using Equation 2 for $R > R_{\text{sp}}$ and $\Omega = \Omega_K(R) = \sqrt{GM/R^3}$, we can write

$$\dot{M}_0\sqrt{GMR}[1 - f(R)] = \dot{J}_0, \quad (5)$$

where

$$f(R) = \frac{3\pi\eta}{\dot{M}} \equiv 1 - \zeta\sqrt{\frac{R_{\text{sp}}}{R}} \quad (6)$$

with $\dot{J}_0 = \zeta \dot{M}_0 \sqrt{GM R_{\text{sp}}}$ and ζ characterizes the dimensionless torque (see Equation 8).

2.3. Propeller Regime

In the quiescent disk solution (Sunyaev & Shakura 1977), sometimes employed for describing the propeller regime (D'Angelo & Spruit 2010; Özsükan et al. 2014), the mass flux in the disk is zero so that the material torque $\dot{M} R^2 \Omega$ vanishes and the viscous stress is alone to balance the magnetic stress at the inner rim of the disk. For such systems the usual Alfvén radius, $r_A \propto \dot{M}^{-2/7}$ becomes irrelevant as it can predict an inner disk radius greater than the light cylinder radius (Özsükan et al. 2014). For super-critical propellers, the mass flux is not totally zero throughout the disk, but still it is reduced heavily at the inner rim so that the inner radius of the disk is to be found by the balance of viscous and magnetic stresses. Being independent of the specific regime (accretion/propeller), the angular momentum balance near the inner disk radius can be expressed as

$$\dot{J}(R_{\text{in}}) - \dot{J}(R_{\text{in}} - \Delta R) = - \int_{R_{\text{in}} - \Delta R}^{R_{\text{in}}} B_\phi^+ B_z R^2 dR, \quad (7)$$

where \dot{J} is the sum of the material and viscous stresses, $B_z \simeq -\mu/R^3$ is the poloidal magnetic field of stellar origin, $B_\phi^+ = \gamma_\phi B_z$ is the toroidal magnetic field above the surface of the disk, and γ_ϕ is the azimuthal pitch factor of order unity. The right-hand side of this equation is of the form $\mu^2 \delta / R_{\text{in}}^3$, where $\delta \equiv \Delta R / R_{\text{in}}$ is the relative width of the coupled domain (boundary region) between the disk and the magnetosphere.

2.3.1. Inner Disk Radius and Spindown Torque

In the propeller regime, material stresses are negligible at R_{in} and the surface density of the disk matter vanishes just inside the innermost disk radius due to the efficient depletion of matter propelled out by the rapidly rotating magnetosphere, i.e., $\eta(R_{\text{in}} - \Delta R) = 0$. This further requires that $\dot{J}(R_{\text{in}} - \Delta R)$ in Equation 7 also vanishes as $\dot{J} \propto \eta$. Using Equation 3 with $\dot{J}_0 = \zeta \dot{M}_0 \sqrt{GM R_{\text{sp}}}$ (see Section 2.2) and $\dot{M}_{\text{in}} = \dot{M}_0 (R_{\text{in}} / R_{\text{sp}})$ for the super-critical regime in Equation 2, we find

$$\dot{J}(R_{\text{in}}) = \zeta \dot{M}_{\text{in}} \sqrt{GM R_{\text{in}}}. \quad (8)$$

As $\dot{J}(R_{\text{in}})$ represents the net torque acting on the neutron star, the integration constant ζ can be identified to be the dimensionless torque. In general, the dimensionless torque, n , is a function of the fastness parameter, $\omega_* \equiv \Omega_* / \Omega_K(R_{\text{in}})$. We, therefore, write the integration constant as $\zeta = n(\omega_*)$. The azimuthal pitch is expected to be proportional to the shear between the magnetosphere and the inner disk matter, i.e.,

$\gamma_\phi \propto \Omega_* - \Omega(R_{\text{in}})$. Accordingly, we choose the dependence of the azimuthal pitch on the fastness parameter as $\gamma_\phi(\omega_*) = \gamma_p(\omega_* - \omega_p)$ for the propeller regime. Here, $\omega_p = \Omega(R_{\text{in}}) / \Omega_K(R_{\text{in}})$ and γ_p are constants of order unity. Next, we substitute Equation 8 into Equation 7 and solve for the innermost disk radius,

$$R_{\text{in}} = \left(\frac{\gamma_p \omega_p \mu^2 R_{\text{sp}} \delta}{n_0 \dot{M}_0 \sqrt{GM}} \right)^{2/9}, \quad (9)$$

for the super-critical propeller regime ($R_{\text{co}} < R_{\text{in}} < R_{\text{sp}}$) assuming that

$$\zeta = n(\omega_*) = n_0 \left(1 - \frac{\omega_*}{\omega_p} \right) \quad (10)$$

in accordance with the dependence of γ_ϕ on ω_* . The propeller (spindown) torque acting on the neutron star can therefore be written as

$$N_p = n_0 \left(1 - \frac{\omega_*}{\omega_p} \right) \dot{M}_{\text{in}} \sqrt{GM R_{\text{in}}}, \quad (11)$$

where n_0 is another proportionality constant of order unity and $\omega_* > \omega_p$.

2.3.2. Luminosity of the Disk with Outflows

The energy budget of propeller systems involves the gravitational potential energy released, L_G , the spindown energy of the neutron star, L_{sd} , and the kinetic energy taken away with the outflowing disk matter, $L_{\text{out}} < 0$. We express the total luminosity as

$$L_{\text{tot}} = L_G + L_{\text{sd}} + L_{\text{out}}. \quad (12)$$

In the subcritical case, this can be written as $L_{\text{tot}} = GMM/R_{\text{in}} - I\Omega_*\dot{\Omega}_* - \frac{1}{2}\dot{M}_{\text{out}}v_{\text{out}}^2$ (see, e.g. Ekşi et al. 2005). Super-critical propellers, however, need further care as the gravitational energy released outside and inside the spherization radius require separate treatment.

For a disk with super-critical mass transfer rates, the rate of potential energy release, $L_G = \int_{R_{\text{in}}}^{R_0} GM\dot{M} dR/R^2$, can be found as

$$L_G = \frac{2}{27\epsilon} \left[\ln \left(\frac{R_{\text{sp}}}{R_{\text{in}}} \right) + 1 - \frac{R_{\text{sp}}}{R_0} \right] L_E \quad (13)$$

where we employed Equation 2.

The energy loss rate due to outflows at the inner region is

$$L_{\text{out}} = \frac{1}{2} \int_{R < R_{\text{sp}}} v_{\text{out}}^2 d\dot{M}_{\text{out}} \quad (14)$$

Using $d\dot{M}_{\text{out}} = -d\dot{M}$ and

$$v_{\text{out}}^2(R) = \frac{2GM}{R} \left(\frac{L_{\text{tot}}}{L_E} - 1 \right) \quad (15)$$

(Shakura & Sunyaev 1973) for $L \geq L_E$, Equation 14 can be evaluated as

$$L_{\text{out}} = -\frac{1}{27\epsilon} \left(\frac{L_{\text{tot}}}{L_E} - 1 \right) \ln \left(\frac{R_{\text{sp}}}{R_{\text{in}}} \right)^2 L_E \quad (16)$$

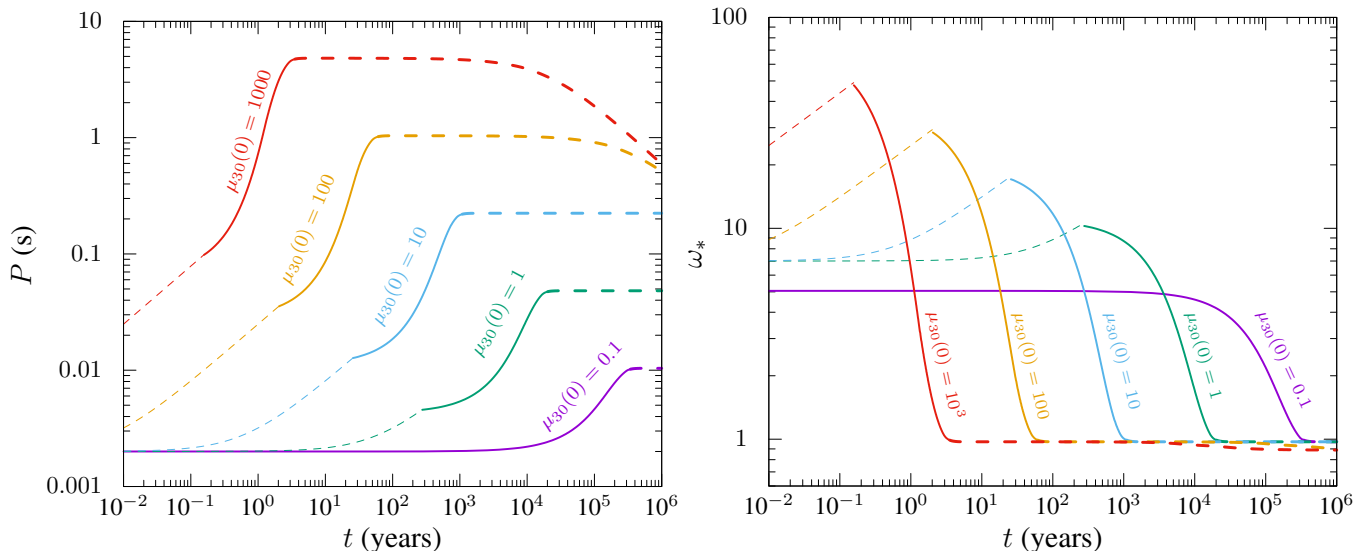


Figure 1. Evolution of the spin period (left panel) and the fastness parameter (right panel) of neutron stars for a variety of initial magnetic fields. The dashed thin lines correspond to the ejector stage, the solid lines correspond to the propeller stage we focus in this work, and the thick dashed lines correspond to the late accretion stage. In all simulations the initial period of the neutron star is taken as $P_0 = 2$ ms, mass flux of $\dot{M}_0 = 4 \times 10^{20} \text{ g s}^{-1}$, and $R_0 = 10^{11}$ cm. The dipole magnetic moments greater than $\mu = 10^{31} \text{ G cm}^3$ are assumed to decay according to the scenario B of Colpi et al. (2000).

where we refer to Equation 2 in the last step.

The spindown power in Equation 12 can be written as

$$L_{\text{sd}} = -N_p \Omega_* = -n(\omega_*) \dot{M}_{\text{in}} \sqrt{GM R_{\text{in}}} \Omega_*. \quad (17)$$

Using ω_* , R_{sp} , and Equation 2, this expression can be further simplified as

$$L_{\text{sd}} = -\frac{2}{27\epsilon} \omega_* n(\omega_*) L_E. \quad (18)$$

The luminosity of the disk interacting with a neutron star at the super-critical propeller regime is finally obtained as

$$\frac{L_{\text{tot}}}{L_E} = \frac{\ln\left(\frac{R_{\text{sp}}}{R_{\text{in}}}\right)^2 + \left(1 - \frac{R_{\text{sp}}}{R_0}\right) - \omega_* n(\omega_*)}{\frac{27\epsilon}{2} + \ln\left(\frac{R_{\text{sp}}}{R_{\text{in}}}\right)}. \quad (19)$$

In the presence of beaming $b < 1$, the luminosity would appear even larger: $L_{\text{obs}} = L_{\text{tot}}/b$.

The total luminosity in the very late super-critical accretion stage is $L_{\text{tot}} = L_G + L_{\text{out}} + L_{\text{acc}}$, where $L_{\text{acc}} = GMM_{\text{in}}/R_*$ is the accretion luminosity for a neutron star of radius R_* .

3. RESULTS

We solved the torque equation, $I\dot{\Omega}_* = N$, by a standard numerical scheme to find the spin and luminosity evolution of neutron stars of moment of inertia I , under super-critical mass inflow.

For the initial magnetic field strengths in the magnetar range, i.e. for $\mu(0) > 10^{31} \text{ G cm}^3$, we allowed

the field decay and employed the mechanism B in Colpi et al. (2000) as an illustrative example. In the slowest field-decay scenario, mechanism A in Colpi et al. (2000), the field strength remains constant throughout the evolutionary timescale leaving the maximum equilibrium period unchanged. For the fastest field-decay scenario, mechanism C in Colpi et al. (2000), the maximum equilibrium period will remain unchanged whereas the asymptotic value of the equilibrium period converges to the equilibrium period attained by $\mu_{30}(0) = 10$ in $\sim 10^6$ yr.

In this work, we focus on the propeller regime and we did not include accretion induced field decay. Our results for the accretion stage would change if accretion induced field decay is considered; e.g. initial magnetic dipole moments even stronger than $\mu_{30}(0) = 10$ would be required to obtain PULX periods. The accretion regime is beyond the scope of this paper and will be studied thoroughly in a subsequent work for different accretion induced field-decay scenarios with additional set of parameters to be scanned for addressing observational properties of PULXs.

For a neutron star of mass $M = 1.4 M_\odot$ and radius $R_* = 10$ km we assumed the initial period $P_0 = 2$ ms, mass flux $\dot{M}_0 = 4 \times 10^{20} \text{ g s}^{-1}$, and the outer disk radius $R_0 = 10^{11}$ cm. We also assumed that $\epsilon = 0.1$, $\delta = 0.01$, $n_0 = 1$, $\omega_p = 0.9$, and $\gamma_p = 0.8$. We obtained results for a range of initial magnetic moments $\mu_{30}(0) = 0.01$, $\mu_{30}(0) = 0.1$, $\mu_{30}(0) = 1$, $\mu_{30}(0) = 10$, $\mu_{30}(0) = 100$, and $\mu_{30}(0) = 1000$, where $\mu_{30}(0) \equiv \mu(t=0)/10^{30} \text{ G cm}^3$. The period and fastness parameter evolution of systems of these systems is shown in Figure 1. We see that systems with

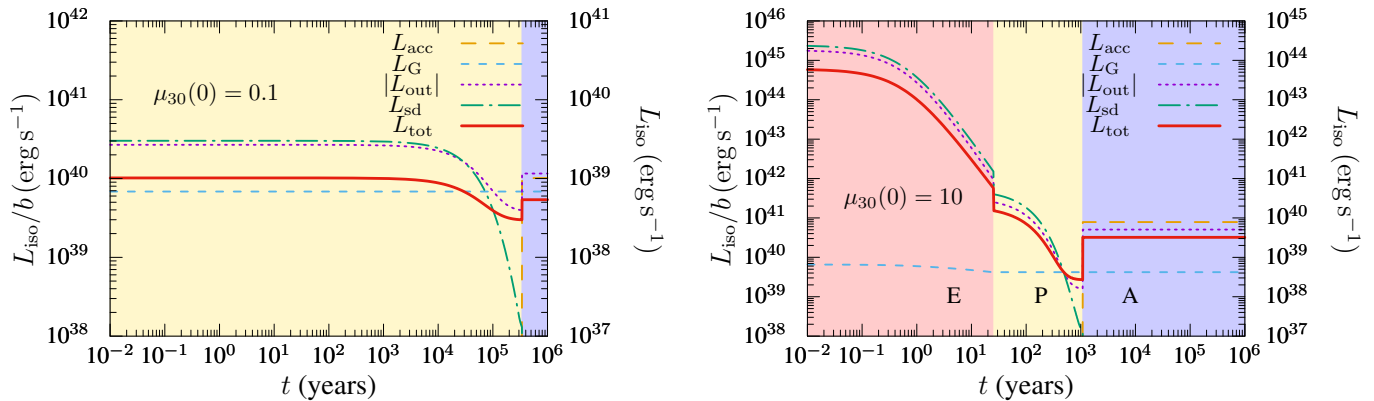


Figure 2. Evolution of the luminosity components of neutron stars for a initial magnetic dipole moment of $\mu_{30}(0) = 0.1$ (left panel) and for $\mu_{30}(0) = 10$ (right panel). As in Figure 1 the initial period of the neutron star is taken as $P_0 = 2$ ms, mass flux of $\dot{M}_0 = 4 \times 10^{20} \text{ g s}^{-1}$, and $R_0 = 10^{11}$ cm. The right vertical axis represents the luminosity for isotropic emission. The observed luminosity given on the left vertical axis is $L_{\text{obs}} = L_{\text{iso}}/b$, where b is assumed to be 0.1. The luminosity enhancement at the late stage ($t \gtrsim 10^5$ yr for the left panel and $t \gtrsim 10^3$ yr for the right panel) corresponds to the super-critical accretion regime where the source might be observed as a PULX. The super-critical propeller regime we focus on in this work corresponds to $t \lesssim 10^5$ yr for the left panel and $t \sim 30 - 1000$ yr for the right panel. In this regime, the source would appear as a nonpulsating ULX. The very early (ejector) phase on the right panel ($t \lesssim 10$ yr) may appear as a supernova impostor. E, P and A labeling differently colored shaded regions denote the ejector, propeller and accretion stages, respectively.

$\mu_{30}(0) < 1$ start in the propeller stage whereas those with $\mu_{30} \geq 1$ start as ejectors. In the ejector stage, the inflowing material does not even reach the light cylinder and the neutron star spins down as an isolated rotating dipole (Lipunov et al. 1992).

The evolution of each luminosity component is shown in Figure 2 for neutron stars with different magnetic fields. The left and right panels show the long-term early-stage evolutions of each luminosity component discussed in the previous section. In line with the period evolution of the same systems with $\mu_{30} = 10$ and $\mu_{30} = 1$ in Figure 1, the neutron stars appear as ULXs for an early period of $10^3 - 10^4$ yr during which they attain their equilibrium period.

As seen from Figure 1, only systems in the range $100 > \mu_{30} > 1000$ have equilibrium periods in the observed range of ~ 1 s. The equilibrium period can be guessed from the torque expression in Equation 11. For $N_p = 0$, $\omega_* = \omega_p \simeq 1$ must be satisfied. This condition yields the equilibrium period, $P_{\text{eq}} \simeq 0.21 \text{ s } \mu_{31}^{2/3} \delta_{0.01}^{1/3}$. Note, however, that longer periods are also possible for wider zones of magnetosphere-disk interaction. In the accretion regime, widths of transition zones as large as 0.6 can be realized (see, e.g. Erkut & Alpar 2004). For $\delta = 0.6$ and $\mu_{31} = 1$, $P_{\text{eq}} \simeq 0.8 \text{ s}$.

4. DISCUSSION AND CONCLUSIONS

We have proposed that some ULX and ULS sources host neutron stars in the super-critical propeller stage corresponding to super-Eddington mass inflow rates and with the radiation pressure in the inner disk sustaining a quasi-spherical geometrically thick structure. This leads to a natural mechanism for the optically thick winds

with velocity $v \sim 0.2c$ launched by radiative and centrifugal processes. The X-ray emission is then processed in this optically thick medium and is observed as soft emission at large viewing angles. The spindown energy released by the slowing down neutron star is the main source of the extreme luminosity of these objects.

We have shown that only those systems with initial magnetic fields $B \gtrsim 10^{13}$ G are spun down to periods $P \sim 1$ s matching the observed periods of PULXs confirming the early view (Ekşi et al. 2015) that the first discovered PULX, M82 X-2 has such strong magnetic fields. Inclusion of accretion induced magnetic field decay will obviously require even stronger initial field strengths. We have estimated the spindown torque and shown that the spindown power at the early stage when the neutron star is rotating rapidly is sufficient to address the luminosity of ULX and ULS systems.

4.1. Evolution from Massive Binaries

We now check that super-Eddington mass inflow rates \dot{M}_0 indicated for ULX evolutionary scenarios are indeed provided by binary evolution, for the required duration of $\sim 10^6$ yr.

In the usual approach to the rotational evolution of neutron stars in massive binaries, prior to the start of accretion, the secular increase of the neutron-star spin period is realized through two successive phases: (i) the ejector phase in which the young neutron star can emit radiation from radio waves to X-rays and (ii) the propeller phase, where the infalling matter of wind from the massive donor is thrown away by the rapidly rotating neutron-star magnetosphere (Illarionov & Sunyaev 1975). In the propeller phase, the system is assumed to

be unobservable or extremely faint in X-rays, because no matter is allowed to accrete onto the neutron-star surface. In the absence of accretion, this assumption can be validated if the spindown power transferred by the neutron-star magnetosphere to the accretion flow remains sufficiently low as for the sub-Eddington mass-inflow rates. The brightest X-ray stage for neutron stars in high-mass X-ray binaries is then anticipated to begin only when the massive component is close to filling its Roche-lobe and starts transferring its mass via an accretion disk (Iben et al. 1995). Once the magnetospheric radius in the inner disk becomes smaller than the corotation radius, the neutron star is said to be X-ray luminous in the so-called accretion phase.

Long before the Roche-lobe overflow occurs, the neutron-star magnetosphere can interact with the wind of the massive companion. In the present evolutionary scheme, we consider the case of a newly born neutron star embedded in the wind of the massive companion. In the earliest stage with neutron-star spin periods of a few milliseconds, the substantial mass transfer to the neutron star can be realized if the donor is an already evolved massive star that is capable of producing dense winds with sufficiently high mass-loss rates. The formation of a helium star–neutron star binary, following an early common-envelope phase in the course of the evolution of two stars of nearly equal initial masses (twin massive binaries), is the best example of a neutron-star birth in a binary where the massive component starts feeding the compact object through powerful winds (Brown 1995; Dewi et al. 2006). The evolution of such binaries usually ends up with double neutron-star systems soon after the explosion of the helium star.

Cygnus X-3 is the only known candidate in our galaxy for a neutron star (or a low-mass black hole) accreting matter from a massive helium star (Wolf–Rayet star; Lommen et al. 2005; Zdziarski et al. 2013). Cygnus X-3, albeit luminous in X-rays ($L_X \simeq 10^{38} \text{ erg s}^{-1}$), is not a ULX. It is, however, possible that Cygnus X-3 represents the late stage of a ULX at which the mass transfer rate has already been reduced to $\dot{M}_0 \simeq \dot{M}_E$. The evolution of helium stars, such as the one in Cygnus X-3, is similar to the evolution of Wolf–Rayet (WR) stars with strong mass loss (McClelland & Eldridge 2016). The typical range for the mass-loss rates due to winds of massive helium/WR stars is $\sim 10^{-6} - 10^{-4} M_\odot \text{ yr}^{-1}$ (Lommen et al. 2005; Crowther 2007; Zdziarski et al. 2013).

Being hot enough, the single hydrogen-poor WR (helium) stars can produce winds with velocities as high as $\sim 4000 \text{ km s}^{-1}$ (Crowther 2007). As revealed by the hydrodynamic atmosphere models for WR stars (Gräfener & Hamann 2005), the radiatively driven wind structure consists of two acceleration regions. The region that is close to the wind base of the stellar atmosphere

is characterized by an optically thick wind of velocities $v_w \lesssim 1000 \text{ km s}^{-1}$. The second region where the wind velocities exceed 1000 km s^{-1} extends across the outer part of the wind. In a close binary, such as Cygnus X-3, the wind velocities can therefore be as low as 1000 km s^{-1} even in the absence of any wind-velocity reduction mechanism.

The observed spectrum of the mass-donor star has been reconstructed in a recent hydrodynamical atmosphere model of the high-mass X-ray binary, Vela X-1 (Sander 2018; Sander et al. 2018). The wind velocity at the location of the neutron star has been estimated as $\sim 100 \text{ km s}^{-1}$, which is much smaller than the typical value of the wind velocity expected according to the standard approach. In the classical Bondi–Hoyle theory, slow wind favors relatively high accretion rates for the wind material (see, e.g., Equation 20). Even if the wind velocities are not as low as the classical theory suggests, the efficiency for the mass transfer through wind accretion may be much higher in X-ray binaries with WR stars than previously thought as in the case of M101 ULX-1 (Liu et al. 2013).

In a high-mass X-ray binary, where the massive donor is X-ray irradiated by the compact X-ray source, the mass transfer can be significantly altered due to the effect of X-ray photoionization of the wind material (Ducci et al. 2010). As revealed by simulations of the stellar wind in X-ray binaries, the X-ray photoionization decelerates the wind matter in the vicinity of the compact object, leads to the formation of an extensive disk, and therefore enhances the overall mass inflow (Čechura & Hadrava 2015). The wind velocities of $\sim 200 \text{ km s}^{-1}$ can be realized if the wind driving radiative processes are suppressed by the effect of X-ray photoionization (Sako et al. 2002). As also mentioned in Section 2, the formation of a disk around the newborn neutron star as an ejector (right panel of Figure 2) or a propeller (left panel of Figure 2) is favored by the reduction of wind velocities due to the X-rays emitted from the young neutron star.

Low wind velocities are not sufficient for the formation of accretion disks around wind-fed compact objects. According to the disk-formation criterion, there is an upper limit for the orbital period of the binary, which depends on the masses of binary components as well in addition to the wind velocity (Lommen et al. 2005). In order to determine the current population of helium star–neutron star (and helium star–black hole) binaries in our galaxy, Lommen et al. (2005) performed a population synthesis and obtained the distribution of core-helium-burning systems in the orbital period versus helium-star mass plane. For a given orbital period and a wind velocity, Lommen et al. (2005) revealed that the disk formation around the neutron star is more likely for massive he-

lium stars with masses $> 7M_\odot$ compared to low-mass helium stars with masses $< 5M_\odot$, though the latter is much more abundant than the former.

The fraction of the mass-loss rate, \dot{M}_w , of the massive helium wind supplier captured by the neutron star is given by

$$\frac{\dot{M}_0}{\dot{M}_w} \simeq 3.2 \times 10^{-3} M_{1.4}^{4/3} P_{1d}^{-4/3} (1+q)^{-2/3} v_{w,1000}^{-4} \quad (20)$$

(see, e.g., [Urpin et al. 1998](#)). Here, $q \equiv M_D/M$ is the mass ratio of the helium star–neutron star binary with M_D being the mass of the helium donor, P_{1d} is the binary orbital period in units of 1 day, $v_{w,1000} \equiv v_w/1000 \text{ km s}^{-1}$ is the wind velocity at the neutron-star location, and $M_{1.4}$ is the neutron-star mass in units of $1.4 M_\odot$. For the mass-transfer rates of $\dot{M}_0 = 4 \times 10^{20} \text{ g s}^{-1}$ ($\simeq 6 \times 10^{-6} M_\odot \text{ yr}^{-1}$) we employ in the present work, the mass-loss rate for the WR star (massive helium donor) with $M_D = 15 M_\odot$ can be estimated using [Equation 20](#) with $v_w = 200 \text{ km s}^{-1}$ as $\dot{M}_w \simeq 1.5 \times 10^{-5} M_\odot \text{ yr}^{-1}$, which is in agreement with the observed mass-loss rates of WR stars ([Zdziarski et al. 2013](#)).

The lifetime of the helium-burning phase for a star of mass $\gtrsim 15 M_\odot$ is $\sim 10^6 \text{ yr}$ ([Hayashi & Cameron 1962](#); [Chiosi et al. 1978](#); [Salasnich et al. 1999](#)). Following the helium burning, the fusion of the carbon, oxygen, and other heavy elements occurs within $\lesssim 10^4 \text{ yr}$ before the donor core collapses into a neutron star. According to our evolutionary scenario, a massive helium star–neutron star binary is left behind an early common-envelope phase during the evolution of two massive main-sequence stars. The accretion disk around the neutron star is fed by the helium-star wind transferred with an average mass flux of $\dot{M}_0 \sim 6 \times 10^{-6} M_\odot \text{ yr}^{-1}$ throughout the helium-burning lifetime. Such a mass-transfer rate can be sustained by the mass-loss rate that evolves in time according to [Equation 20](#). Noting that $\dot{M}_w = -dM_D/dt$ and using typical values such as $M_{1.4} = 1 = P_{1d}$ and $v_{w,1000} = 0.2$ for all quantities except M_D as a simplifying assumption, it follows from the integration of [Equation 20](#) over 10^6 yr that the terminal mass of the helium star toward the end of helium-burning phase (before carbon burning starts) is $\sim 4 M_\odot$ for an initial helium-star mass of $15 M_\odot$ (at the onset of helium burning) if mass-inflow rates are super-Eddington with $\dot{M}_0 \sim 6 \times 10^{-6} M_\odot \text{ yr}^{-1}$ as appropriate for ULX. The evolutionary scenario we presently invoke to explain a subgroup of ULXs (such as the ULS and some nonpulsating ULX) cannot, however, account for the observed population of X-ray binaries with low-mass helium stars. Instead, the majority of systems with low-mass helium stars are likely to be the direct outcome of an early common-envelope phase in the course of the

evolution of two massive stars ([Bhattacharya & van den Heuvel 1991](#)).

The chemical composition of the wind-fed disk around the neutron star is determined by the ingredients of the helium-star envelope. In case all hydrogen is depleted, a helium-rich disk with the same critical rate of mass inflow can be realized provided $(L_E/\epsilon)_{\text{He}} = (L_E/\epsilon)_{\text{H}}$. The Eddington luminosity for the accretion of the helium-rich matter is twice the Eddington luminosity for the hydrogen-rich gas. The efficiency of the helium-rich disk is then $\epsilon_{\text{He}} = 2\epsilon_{\text{H}} \simeq 0.2$ for $\epsilon_{\text{H}} \simeq 0.1$ ([Section 2](#)). It is possible to compare the luminosities of the helium- and hydrogen-rich disks assuming the same numerical values for all model parameters except ϵ . Note from [Equation 13](#) and [Equation 17](#) that $(L_G)_{\text{He}} = (L_G)_{\text{H}}$ and $(L_{\text{sd}})_{\text{He}} = (L_{\text{sd}})_{\text{H}}$. Using [Equation 19](#), on the other hand, we find

$$\frac{(L_{\text{tot}})_{\text{He}}}{(L_{\text{tot}})_{\text{H}}} = 1 + \left[1 + \frac{27\epsilon_{\text{H}}}{\ln(R_{\text{sp}}/R_{\text{in}})} \right]^{-1}. \quad (21)$$

As seen from [Equation 21](#), $(L_{\text{tot}})_{\text{He}} \simeq (L_{\text{tot}})_{\text{H}}$ for $R_{\text{sp}}/R_{\text{in}} \simeq 1$, which can be satisfied for sufficiently strong magnetic fields. For magnetic fields as low as 10^{11} G in strength, $R_{\text{sp}}/R_{\text{in}} \simeq 80$ and $(L_{\text{tot}})_{\text{He}} \simeq 1.6(L_{\text{tot}})_{\text{H}}$. The difference between the helium- and hydrogen-rich disk luminosities is therefore negligible throughout the evolutionary lifetime (10^6 yr) as far as the ULX luminosity range is concerned, so that our scenario is not sensitive to composition.

4.2. Neutron Stars Rather than Black Holes

Given the abundance of neutron stars over black holes as the outcome of stellar evolution, it was proposed that the bulk of the ULX population may consist of neutron stars in binary systems rather than accreting stellar-mass black holes ([Fragos et al. 2015](#); [Shao & Li 2015](#); [King et al. 2017](#); [Middleton & King 2017](#); [Wiktorowicz et al. 2017](#)). Because of the large mass ratio in a neutron-star high-mass X-ray binary, however, the mass transfer is not stable unlike the black hole systems, where Roche-lobe overflow is stable rendering such sources relatively long-lived as compared to their neutron-star counterparts and thus strong candidates for nonpulsating ULX ([Rappaport et al. 2005](#)).

The support in favor of neutron stars being dominant in the ULX population is provided by [Pintore et al. \(2017\)](#) who show that some of the nonpulsating ULXs they studied exhibit similar X-ray spectra with PULXs. Specifically, 2 of the 12 sources analyzed by [Pintore et al. \(2017\)](#) show the hard power-law with exponential cutoff component that is likely associated with the accretion column and are thus likely to be accreting sources. The lack of pulsations from these systems could be due to an optically thick medium smearing out the pulsations

(Ekşi et al. 2015; Mushtukov et al. 2017). For the rest of the sources that lack the hard component and have softer spectra, the super-critical propeller regime that we consider in this work cannot be excluded. ULS' are likely to be super-critical propeller systems with lower magnetic dipole moments, $\mu \sim 10^{29}$ G cm³ (see the left panel of Figure 2) given that the propeller stage of these systems has a longer life-time. Such low-B systems at the accretion stage will have spin periods as small as $P \sim 10$ ms yet may not show pulsations as their magnetosphere enshrouded by super-Eddington accretion is very small.

In the presence of beaming the characteristic spin-down time-scale becomes

$$\tau_c = 3.1 \times 10^6 \text{ yr } b_{0.01}^{-1} L_{40,\text{iso}}^{-1} P_{2\text{ms}}^{-2} I_{45} \quad (22)$$

where $b_{0.01} = b/0.01$ is the beaming fraction in units of 0.01, $P_{2\text{ms}} = P_0/(2\text{ms})$ and $L_{40,\text{iso}}$ is the isotropic luminosity in units of 10^{40} erg s⁻¹. This shows that at least 10% of the NS population of the ULX/ULS systems that evolve from neutron star–helium star binaries could be in the supercritical propeller stage with duration $\lesssim 10^5$ yr (Figure 2) if the evolutionary timescale is $\sim 10^6$ yr.

The first discovered PULX M82 X-2 is known to show bimodal luminosity behavior in the archival data (Tsygankov et al. 2016). The authors interpret the low-luminosity stage as an evidence for the transition of the source to the propeller regime. We find it necessary to emphasize that this propeller stage is distinct from the early super-Eddington propeller phase we consider in this work, as the neutron star in this system has already

slowed down to $P \sim 1$ s and the spindown power is no longer sufficient for making the object appear ultra-luminous in the observed late propeller stage.

A final note is about the anomalous X-ray pulsar (AXP) 4U 0142+61. A supernova fallback disk is detected in this system by Wang et al. (2006) and likely around 1E 2259+586 (Kaplan et al. 2009), which also is an AXP. Such disks were proposed to exist around young pulsars (Michel & Dessler 1981) at a time when AXPs had not been identified. Later on they were proposed as an alternative to the magnetar picture (Chatterjee et al. 2000; Alpar 2001) and as an ingredient of magnetars with strong magnetic fields in multipoles (Ekşi & Alpar 2003; Ertan & Alpar 2003). Whether the detected disk is passive (Wang et al. 2006) or active, as is likely (Ertan et al. 2007), at the present time, it must have been highly active at its earliest stages with super-critical mass inflow passing through a super-critical propeller stage (Ekşi & Alpar 2003; Yan et al. 2012) and must have been as bright as an ULX/ULS system. This implies that some fraction of ULX or ULS systems though not in binary systems could form super-critical propeller systems with the supernova fallback disks and form the progenitors of AXPs and other classes of young neutron stars.

ACKNOWLEDGMENTS

M.H.E. acknowledges the post-doctoral research support from the BAP unit of Istanbul Technical University. M.A.A. is a member of the Science Academy (Bilim Akademisi), Turkey.

REFERENCES

- Alpar, M. A. 2001, *ApJ*, 554, 1245
 Anzer, U., Boerner, G., & Monaghan, J. J. 1987, *A&A*, 176, 235
 Bachetti, M., Harrison, F. A., Walton, D. J., et al. 2014, *Nature*, 514, 202
 Bhattacharya, D., & van den Heuvel, E. P. J. 1991, *PhR*, 203, 1
 Brown, G. E. 1995, *ApJ*, 440, 270
 Carpano, S., Haberl, F., Maitra, C., & Vasilopoulos, G. 2018, *MNRAS*, 476, L45
 Chatterjee, P., Hernquist, L., & Narayan, R. 2000, *ApJ*, 534, 373
 Chiosi, C., Nasi, E., & Sreenivasan, S. R. 1978, *A&A*, 63, 103
 Colpi, M., Geppert, U., & Page, D. 2000, *ApJL*, 529, L29
 Crowther, P. A. 2007, *ARA&A*, 45, 177
 D'Angelo, C. R., & Spruit, H. C. 2010, *MNRAS*, 406, 1208
 Dewi, J. D. M., Podsiadlowski, P., & Sena, A. 2006, *MNRAS*, 368, 1742
 Di Stefano, R., & Kong, A. K. H. 2003, *ApJ*, 592, 884
 Ducci, L., Sidoli, L., & Paizis, A. 2010, *MNRAS*, 408, 1540
 Ekşi, K. Y., & Alpar, M. A. 2003, *ApJ*, 599, 450
 Ekşi, K. Y., Andaç, İ. C., Çikintoğlu, S., et al. 2015, *MNRAS*, 448, L40
 Ekşi, K. Y., Hernquist, L., & Narayan, R. 2005, *ApJL*, 623, L41
 Erkut, M. H., & Alpar, M. A. 2004, *ApJ*, 617, 461
 Ertan, Ü., & Alpar, M. A. 2003, *ApJL*, 593, L93
 Ertan, Ü., Erkut, M. H., Ekşi, K. Y., & Alpar, M. A. 2007, *ApJ*, 657, 441
 Fabbiano, G., King, A. R., Zezas, A., et al. 2003, *ApJ*, 591, 843
 Feng, H., Tao, L., Kaaret, P., & Grisé, F. 2016, *ApJ*, 831, 117
 Fragos, T., Linden, T., Kalogera, V., & Sklias, P. 2015, *ApJL*, 802, L5
 Fürst, F., Walton, D. J., Harrison, F. A., et al. 2016, *ApJL*, 831, L14
 Gräfener, G., & Hamann, W.-R. 2005, *A&A*, 432, 633
 Hayashi, C., & Cameron, R. C. 1962, *ApJ*, 136, 166
 Iben, Jr., I., Tutukov, A. V., & Yungelson, L. R. 1995, *ApJS*, 100, 217
 Illarionov, A. F., & Sunyaev, R. A. 1975, *A&A*, 39, 185
 Israel, G. L., Belfiore, A., Stella, L., et al. 2017a, *Science*, 355, 817
 Israel, G. L., Papitto, A., Esposito, P., et al. 2017b, *MNRAS*, 466, L48
 Kaplan, D. L., Chakrabarty, D., Wang, Z., & Wachter, S. 2009, *ApJ*, 700, 149
 King, A., Lasota, J.-P., & Kluźniak, W. 2017, *MNRAS*, 468, L59
 King, A. R., Davies, M. B., Ward, M. J., Fabbiano, G., & Elvis, M. 2001, *ApJL*, 552, L109
 Kong, A. K. H., & Di Stefano, R. 2003, *ApJL*, 590, L13
 Kylafis, N. D., & Xilouris, E. M. 1993, *A&A*, 278, L43

- Lipunov, V. M. 1982, *Soviet Ast.*, 26, 54
 —. 1987, *Ap&SS*, 132, 1
- Lipunov, V. M., Börner, G., & Wadhwa, R. S. 1992, *Astrophysics of Neutron Stars* (Springer), 108
- Lipunova, G. V. 1999, *Astronomy Letters*, 25, 508
- Liu, J.-F., Bregman, J. N., Bai, Y., Justham, S., & Crowther, P. 2013, *Nature*, 503, 500
- Livio, M., Soker, N., de Kool, M., & Savonije, G. J. 1986, *MNRAS*, 222, 235
- Lommen, D., Yungelson, L., van den Heuvel, E., Nelemans, G., & Portegies Zwart, S. 2005, *A&A*, 443, 231
- Lovelace, R. V. E., Romanova, M. M., & Bisnovatyi-Kogan, G. S. 1999, *ApJ*, 514, 368
- Lü, G.-L., Zhu, C.-H., & Wang, Z.-J. 2011, *Research in Astronomy and Astrophysics*, 11, 327
- McClelland, L. A. S., & Eldridge, J. J. 2016, *MNRAS*, 459, 1505
- Michel, F. C., & Dessler, A. J. 1981, *ApJ*, 251, 654
- Middleton, M. J., & King, A. 2017, *MNRAS*, 470, L69
- Mineshige, S., Rees, M. J., & Fabian, A. C. 1991, *MNRAS*, 251, 555
- Mushtukov, A. A., Suleimanov, V. F., Tsygankov, S. S., & Ingram, A. 2017, *MNRAS*, 467, 1202
- Özsükan, G., Ekşi, K. Y., Hambaryan, V., et al. 2014, *ApJ*, 796, 46
- Pinto, C., Alston, W., Soria, R., et al. 2017, *MNRAS*, 468, 2865
- Pintore, F., Zampieri, L., Stella, L., et al. 2017, *ApJ*, 836, 113
- Poutanen, J., Lipunova, G., Fabrika, S., Butkevich, A. G., & Abolmasov, P. 2007, *MNRAS*, 377, 1187
- Rappaport, S. A., Podsiadlowski, P., & Pfahl, E. 2005, *MNRAS*, 356, 401
- Sako, M., Kahn, S. M., Paerels, F., et al. 2002, in *High Resolution X-ray Spectroscopy with XMM-Newton and Chandra*, ed. G. Branduardi-Raymont, 36
- Salasnich, B., Bressan, A., & Chiosi, C. 1999, *A&A*, 342, 131
- Sander, A. A. C. 2018, arXiv e-prints, arXiv:1811.03106
- Sander, A. A. C., Fürst, F., Kretschmar, P., et al. 2018, *A&A*, 610, A60
- Shakura, N. I., & Sunyaev, R. A. 1973, *A&A*, 24, 337
- Shao, Y., & Li, X.-D. 2015, *ApJ*, 802, 131
- Sunyaev, R. A., & Shakura, N. I. 1977, *Pisma v Astronomicheskii Zhurnal*, 3, 262
- Tsygankov, S. S., Mushtukov, A. A., Suleimanov, V. F., & Poutanen, J. 2016, *MNRAS*, 457, 1101
- Urpin, V., Kononov, D., & Geppert, U. 1998, *MNRAS*, 299, 73
- Urquhart, R., & Soria, R. 2016, *MNRAS*, 456, 1859
- Čechura, J., & Hadrava, P. 2015, *A&A*, 575, A5
- Wang, Z., Chakrabarty, D., & Kaplan, D. L. 2006, *Nature*, 440, 772
- Wiktorowicz, G., Sobolewska, M., Lasota, J.-P., & Belczynski, K. 2017, *ApJ*, 846, 17
- Wiktorowicz, G., Sobolewska, M., Sądowski, A., & Belczynski, K. 2015, *ApJ*, 810, 20
- Yan, T., Perna, R., & Soria, R. 2012, *MNRAS*, 423, 2451
- Zdziarski, A. A., Mikołajewska, J., & Belczyński, K. 2013, *MNRAS*, 429, L104